Improvement in Tribological Properties by Modification of Grain Boundary and Microstructure of Ultrananocrystalline Diamond Films

Kamatchi Jothiramalingam Sankaran,[†] Niranjan Kumar,[§] Joji Kurian,[‡] Radhika Ramadoss,[⊥] Huang-Chin Chen,[‡] Sitaram Dash,[§] Ashok Kumar Tyagi,[§] Chi-Young Lee,[†] Nyan-Hwa Tai,*,[†] and I-Nan Lin*,[‡]

[†]Department of Materials Science and Engineering, National Tsing-Hua University, Hsinchu 300, Taiwan, Republic of China
[§]Materials Science Group, Indira Gandhi Centre for Atomic Research, Kalpakkam 603 102, India
[‡]Department of Physics, Tamkang University, New-Taipei 251, Taiwan, Republic of China
[⊥]Crystal Growth Centre, Anna University, Chennai 600 025, India

ABSTRACT: Grain boundaries and microstructures of ultrananocrystalline diamond (UNCD) films are engineered at nanoscale by controlling the substrate temperature (T_S) and/or by introducing H_2 in the commonly used Ar/CH_4 deposition plasma in a microwave plasma enhanced chemical vapor deposition system. A model for the grain growth is proposed. The films deposited at low T_S consist of random/spherical shaped UNCD grains with well-defined grain boundaries. On increasing T_S, the adhering efficiency of CH radical onto diamond lattice drops and *trans*-polyacetylene (*t*-PA) encapsulating the nanosize diamond clusters break due to hydrogen abstraction activated, rendering the diamond phase less passivated. This leads to the C_2 radical further attaching to the diamond lattice, resulting in the modification of grain boundaries and promoting larger sized clustered grains with a complicated defect structure. Introduction of H_2 in the

plasma at low T_S gives rise to elongated clustered grains that is attributed to the presence of atomic hydrogen in the plasma, preferentially etching out the *t*-PA attached to nanosized diamond clusters. On the basis of this model a technologically important functional property, namely tribology of UNCD films, is studied. A low friction of 0.015 is measured for the film when ultranano grains are formed, which consist of large fractions of grain boundary components of sp^2/a-C and *t*-PA phases. The grain boundary component consists of large amounts of hydroxylic and carboxylic functional groups which passivates the covalent carbon dangling bonds, hence low friction coefficient. The improved tribological properties of films can make it a promising candidate for various applications, mainly in micro/nanoelectro mechanical system (M/NEMS), where low friction is required for high efficiency operation of devices.

KEYWORDS: ultrananocrystalline diamond films, microstructure, grain boundary, clustered grains, trans-polyacetylene, high resolution transmission electron microscopy, tribological properties
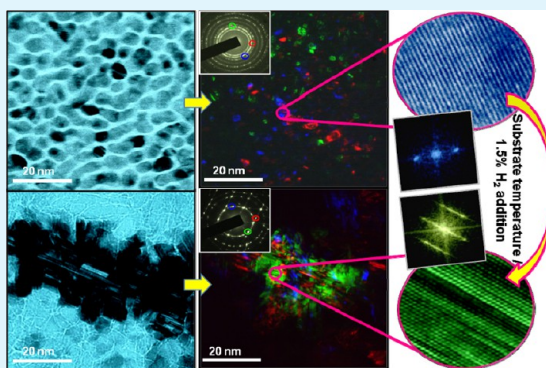
1. INTRODUCTION

Thin diamond films, known to be highly thermally conductive, chemically inert, mechanically hard, and highly elastic, are characterized by a low friction coefficient. In addition, they are highly insulating and possess a low coefficient of thermal expansion. The possibilities that this material presents for surface acoustic devices[1,2] and microelectromechanical devices are immense.[3,4] Among diamond films, ultrananocrystalline diamond (UNCD) films with distinctive microstructural features have received a lot of attention from researchers over the past decade.[5−10] The exceptional characteristics of UNCD are related to volume fraction of the grain boundary phase, which increases as grain size decreases, something that occurs to a greater extent in UNCD than in nano- and microcrystalline diamond films. The grains in the UNCD films are of ultrasmall sizes (up to 10 nm) leading to relatively smooth surface but still

bring about an improvement in the electron field emission and electronic properties as well as mechanical properties such as hardness and elastic modulus which is almost similar to that of pure diamond.[8−16] The moderate hardness and elastic modulus of nanocrystalline diamond (NCD) films exhibit high wear resistance and low friction coefficient.[17,18] A significantly low friction coefficient is observed when the grain boundary volume fraction of NCD films, which consists of lubricant phases of amorphous carbon (a-C) and sp^2 bonded graphite, increases.[19,20] Chemical passivation of the surface is also required to obtain low friction.[21,22] Several unique properties of UNCD films may find potential applications as low friction, hard, and
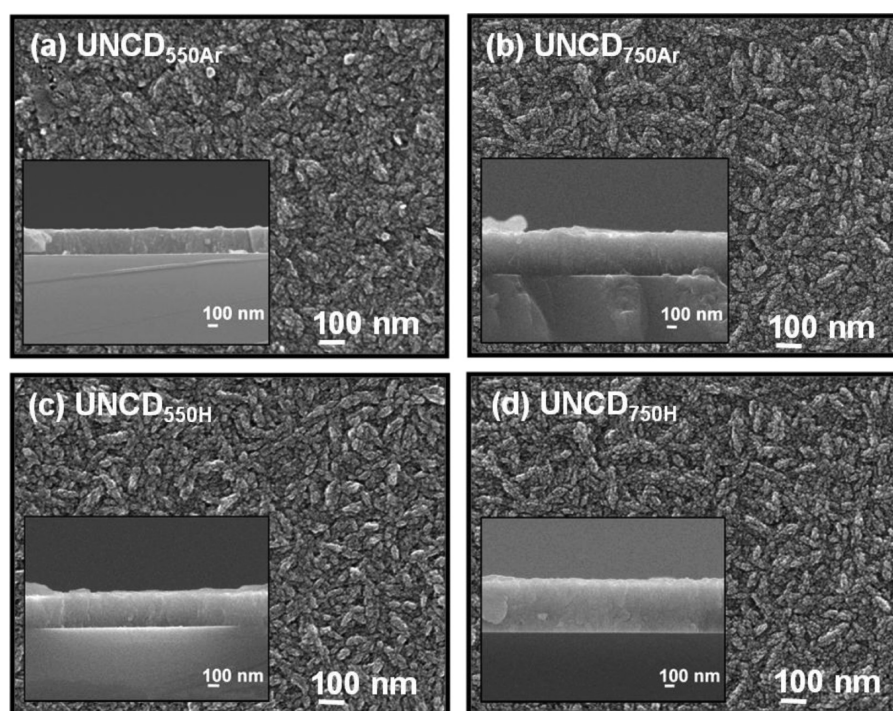
Figure 1. Top-view FESEM images (insets shows the corresponding cross-section FESEM images) of (a) $UNCD_{550Ar}$, (b) $UNCD_{750Ar}$, (c) $UNCD_{550H}$, and (d) $UNCD_{750H}$.

protective wear-resistant coating materials, robust conducting coating for electrochemical electrodes[23] and biocompatible and biologically active substrates.[24]

The microstructure of UNCD films is extremely sensitive to the film deposition parameters like the reactant gas ratio, plasma content, substrate temperature (T_S), etc. Hydrogen has long been considered a vital plasma constituent for the growth of UNCD films using the chemical vapor deposition (CVD) technique under specific conditions of T_S, chamber pressure, etc.[16] It is a key reactant in diamond deposition, its utility ranging from etching away of any growing sp^2-bonded nuclei and stabilization of the surface of growing diamond nuclei to the abstraction of surface hydrogen and assisting in affording a reactive site for methyl radical absorption.[25] The manner in which nucleation occurs may differ with a difference in the hydrogen content, altering the microstructure of conventional diamond films.[26−28] UNCD films synthesized with Ar/CH_4 plasma, on the other hand, exhibit lesser temperature-dependent growth. This is in spite of an increase in growth rate, which is a thermally activated process, with increasing T_S.[29,30] Introduction of hydrogen in Ar/CH_4 plasma gives rise to dendritic shaped grains, with the area occupied by dendritic grains increasing with hydrogen content in the plasma.[31−34] While such studies report the formation of dendritic shaped grains, a change in the other deposition parameters can influence/alter the grain growth mechanism too.

This paper presents synthesis of UNCD films in two different plasma gas mixtures of Ar/CH_4 and Ar/1.5% H_2/CH_4 at various T_S (550−750 °C). The field emission scanning electron microscopy (FESEM), visible-Raman spectroscopy, and transmission electron microscopy (TEM) studies demonstrate how T_S and addition of hydrogen to the Ar/CH_4 plasma influence the microstructure formation and variation in the chemical species such as the different hybridized carbon phases and networking of the *trans*-polyacetylene (*t*-PA) segments in the films. On the basis of these studies, the plasma chemistry and T_S dependent model of microstructure and grain growth mechanism is proposed. The variation in grain/grain boundary microstructure and chemical characteristics of the films is correlated with the tribological properties.

2. EXPERIMENTAL METHODS

A microwave plasma enhanced chemical vapor deposition (MPECVD) system (2.45 GHz 6 in. IPLAS-CYRANNUS) was employed for the deposition of UNCD films. Two series of UNCD films were grown on n-type silicon substrates, each grown by 1 h of deposition. Prior to the deposition of UNCD films, the substrates were preseeded by ultrasonic abrasion for 45 min in a methanol solution containing nanodiamond powder (∼5 nm in size) and titanium powder (SIGMA-Aldrich) (365 mesh) to create nucleation sites necessary for growing the films. For the first series, the reactant gas ratio was maintained as Ar/CH_4 = 99/1 with the input microwave power = 1200 W and pressure = 120 Torr. The films were grown at T_S ranging from 550 to 750 °C, maintaining the temperature constant using a heater attached below the substrate. The corresponding films were designated as $UNCD_{nAr}$, where n is the T_S. For the second series, 1.5% of H_2 was added to the Ar/CH_4 plasma (Ar/H_2/CH_4 = 97.5/1.5/1) and the films were grown at 1200 W and 110 Torr. The T_S was varied between 550 and 750 °C, designating the films obtained as $UNCD_{nH}$, where n is the T_S.

Morphological, structural, and crystallographic characterizations of the UNCD films were carried out with FESEM (JEOL-6500F) and TEM (JEOL-2100F). The bonding structure of the films was investigated by visible-Raman spectroscopy (Lab Raman HR800, Jobin Yvon; λ = 632 nm). Fourier transformed infrared (FTIR) absorbance spectra with 4 cm^{-1} resolution were obtained at normal incidence in an evacuated chamber of an IFS 66 V FTIR spectrometer, Bruker Optics. A KBr beam splitter and a DTGS detector with KBr window were used to follow the frequency range 700−5000 cm^{-1}. In order to attain information on plasma species during the deposition process, optical emissions were measured using optical emission spectroscopy (OES). Rotational mode of a ball on disk nano-tribometer, NTR[2] (CSM Instruments, Switzerland) was used to carry
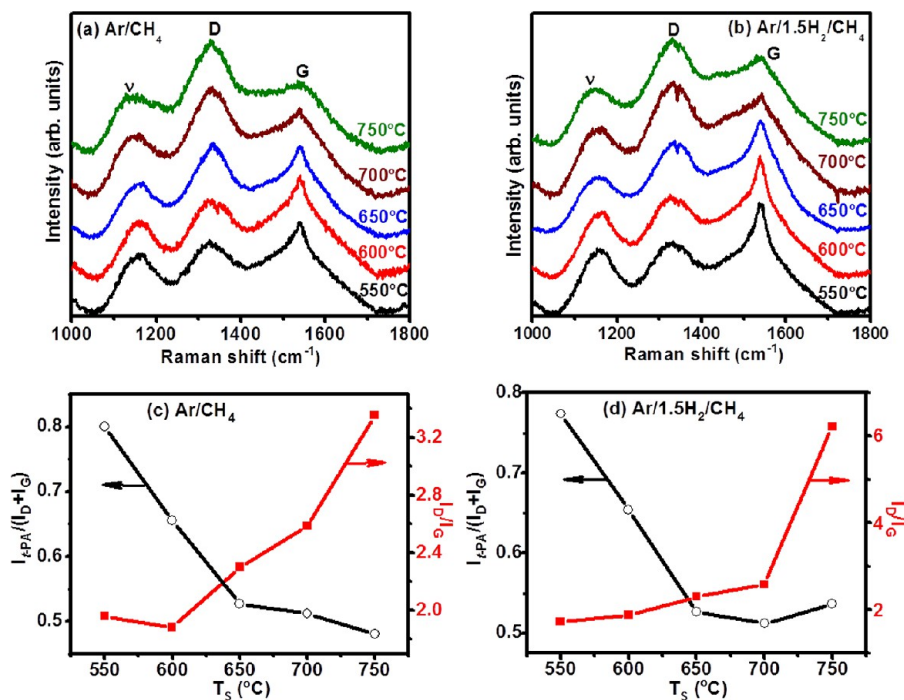
Figure 2. T_S dependence of visible-Raman spectra of UNCD films deposited in (a) Ar/CH$_4$ plasma and (b) Ar/1.5% H$_2$/CH$_4$ plasma. $I_{t\text{-PA}}/(I_D + I_G)$ and I_D/I_G of UNCD films deposited in (c) Ar/CH$_4$ plasma and (d) Ar/1.5% H$_2$/CH$_4$ plasma, where $I_{t\text{-PA}}$, I_D, and I_G are the integrated intensities of the ($\nu_1 + \nu_3$), D-band, and G-band peaks, respectively.

out tribological tests of these films in ambient atmosphere and room temperature. Residual relative humidity in the test chamber was 52%. The contacting steel (100Cr6) ball sliding against the static specimen was 1.5 mm in diameter. Sliding speed of the specimen against the ball and normal load were kept constant at 0.5 cm/s and 50 mN, respectively. The total sliding distance for each measurement was kept constant at 5 m. Each tribological experiment was performed two times and the data was found to be within an error of 5%.

3. RESULTS AND DISCUSSION

3.1. Materials Characterization. *3.1.1. Field Emission Scanning Electron Microscopy Studies.* The comparative morphology and microstructure of UNCD films obtained for the lowest and highest T_S used is shown in Figure 1. The top-view FESEM image of UNCD$_{550Ar}$ shows random/spherical structure of grains in the films (Figure 1a), while that for UNCD$_{750Ar}$ shows slightly larger and elongated grains (Figure 1b). The corresponding cross-sectional FESEM images (insets of Figures 1a and b) show that higher T_S results in higher growth rate (UNCD$_{550Ar}$ = 260 nm/h, UNCD$_{750Ar}$ = 465 nm/h). Figure 1c depicts the top-view FESEM image of UNCD$_{550H}$ showing grains almost comparable to the size of those seen in the UNCD$_{750Ar}$ films, while the grains of the UNCD$_{750H}$ (Figure 1d) are much larger in size compared to that of UNCD$_{550H}$ (UNCD$_{750Ar}$), with indications of greater lateral dimensional growth of grains. This indicates that the T_s dependent growth rate of the UNCD$_{nH}$ films too follows the same trend as that of UNCD$_{nAr}$ films which is observed from the corresponding cross-sectional FESEM images (insets of Figures 1c and d). The higher T_S results in higher growth rate of 350 nm/h = UNCD$_{550H}$ and 520 nm/h = UNCD$_{750H}$. The apparent changes in the morphology of the films seen in the FESEM images occurs with change in T_S as well as change in the reactant gas contentthat results in different carbon phases existing in the films.

3.1.2. Visible-Raman Spectroscopy Studies. Raman spectroscopy is an important technique to explore the different carbon phases present in the films deposited with changes in the reactant gas content as well as T_S. Figure 2a and b show, respectively, the visible-Raman spectra of the samples deposited in the Ar/CH$_4$ and Ar/1.5% H$_2$/CH$_4$ plasma at different T_S. Three prominent broad peaks are observed in the spectra for both sets of films. There is ν_1 ($\sim$1140 cm^{-1}), which originates due to the vibration of *trans*-polyacetylene (*t*-PA) segments present at the grain boundaries.[35,36] Another peak, called the breathing modes of the D-band ($\sim$ 1330 cm^{-1}) is attributed to the disorder-activated aromatic modes of A_{1g} symmetry that involves phonons near the K zone boundary.[37] A stretching mode appears in aromatic rings of G-band ($\sim$1540 cm^{-1}) pertaining to the Brillouin/optical zone center vibrations of E_{2g} mode in the sp^2 bond present at the grain boundaries.[38–42] The broad peaks are suggestive of the small size of grains in the films. A small kink is observed at $\sim$1475 cm^{-1}. This kink designated as ν_3 which is also assigned to contributions from *trans*-polyacetylene (*t*-PA) segments present at the grain boundaries.[35,36] When the T_S is raised the overall intensity of the diamond peak and *t*-PA bands slightly decreases, possibly due to the decrease in noncubic diamond contents and/or the decrease in thickness of the films.[43] Figures 2c and d show the variation of $I_{t\text{-PA}}/(I_D + I_G)$ and I_D/I_G of the films with T_S, where $I_{t\text{-PA}}$, I_D, and I_G are the integrated intensities, taken after normalization of the resonance peaks, of the ν_1, ν_3, D-band, and G-band peaks, respectively. For both the series of samples, the $I_{t\text{-PA}}/(I_D + I_G)$ ratio decreases with T_S. This indicates that the net amount of *t*-PA decreases relative to the amount of the other sp^2 bonded carbon phases in the films as T_S increases. This shows that the T_S plays an important role in determining the changes of *t*-PA and other sp^2 content in the films. The degree of disorder or graphitization of the clustered sp^2 bonded carbon phase in the films is inferred from the I_D/I_G ratio.[28,44] In

3616

dx.doi.org/10.1021/am303144m | *ACS Appl. Mater. Interfaces* 2013, 5, 3614−3624

both the sets of films the I_D/I_G ratio increases with increasing T_S, indicating the lesser graphitization of the samples or lesser sp^2 bonding with increasing T_S.[45,46]

3.1.3. Fourier Transformed Infrared Spectroscopy Studies.

Investigation of functional bonding state on the surface is one of the important aspects to describe the chemical nature and surface energy. In this respect, the FTIR spectra are obtained from the $UNCD_{550Ar}$, UNC_{750Ar}, $UNCD_{550H}$, and $UNCD_{750H}$ films as shown in Figure 3a–d, respectively. All the films show
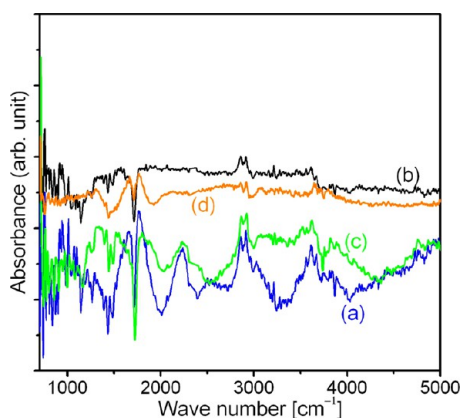
Figure 3. FTIR spectra of (a) $UNCD_{550Ar}$, (b) $UNCD_{750Ar}$, (c) $UNCD_{550H}$, and (d) $UNCD_{750H}$ films. All the films show absorption bands at 1772 cm^{-1}, which corresponds to chemical species C=O, as well as several bands in the region 1017−1363 cm^{-1}, which are assigned to the C—O—C stretching vibration.

an absorption band at 1772 cm^{-1}, which corresponds to chemical species C=O, as well as several bands in the region 1017−1363 cm^{-1}, which are assigned to the C—O—C stretching vibration.[47−49] The presence of these bands suggests that the diamond surface reacted with oxygen in the environment readily. The intensity of these bands is rather strong in $UNCD_{550Ar}$ and $UNCD_{550H}$ films (Figure 3a and c) as compared to $UNCD_{750Ar}$ and $UNCD_{750H}$ film (Figure 3b and d). The intensity of these bands is rather strong in the $UNCD_{550Ar}$ film (Figure 3a) as compared to the $UNCD_{750Ar}$ film (Figure 3b). The absorption band at 1640 cm^{-1} is due to physically absorbed water molecules.[48,49] This band is stronger in $UNCD_{550Ar}$ and $UNCD_{550H}$ films which corresponds to more reactive sites. It is observed that the atmospheric oxygen and hydrogen molecules basically occupy the grain boundary of the diamond crystallites. The grain boundary volume fraction increases when crystallite size decreases. With increase in grain boundary volume fraction, the adsorption of such molecules increases. Further, diamond crystallites contain sp^3 C—C hybridized bonding state and sp^2 C—C/a-C network in the grain boundaries. Oxygen and hydrogen molecules predominantly affect the grain boundaries since the existence of a dangling bond is high. Several absorption bands are observed in the spectral range of 2800−3100 cm^{-1} which arises from C—H stretching vibrations.[47,49] In this region, two peaks are present at 2852 and 2930 cm^{-1}. These are symmetric and antisymmetric stretching vibrations of sp^3 CH$_3$ and sp^3 CH$_2$ group, respectively. Thus, the intensity of these bands is rather strong in $UNCD_{550Ar}$ and $UNCD_{550H}$ films (Figure 3a and c). The C—H vibrational frequencies are assigned according to the carbon hybridization state. This suggests that hydrogen is
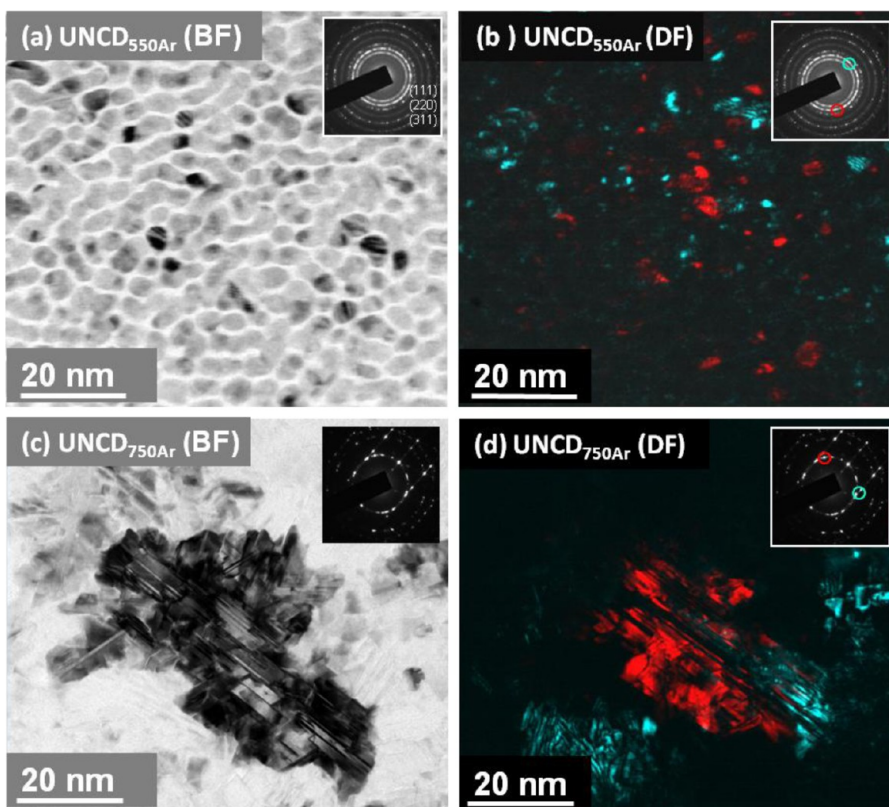

Figure 4. (a) Bright field (BF) and (b) dark field (DF) TEM images of $UNCD_{550Ar}$. (c) BF-TEM and (d) DF-TEM images of $UNCD_{750Ar}$. The insets show the corresponding SAED patterns of each image.

3617

dx.doi.org/10.1021/am303144m | ACS Appl. Mater. Interfaces 2013, 5, 3614−3624

incorporated basically on noncrystalline or defective regions of the film. The defect increases with increase in grain boundary volume fraction. It is rather high in $UNCD_{550Ar}$ and $UNCD_{550H}$ films. Further, the peak at 1465 and 1090 cm^{-1} corresponds to C=C aromatic stretching and O—CH_3 deformation mode, respectively.[47,48] In addition, peaks at 890 and 1223 cm^{-1} are assigned to the bending of sp^3 C—C hybridized C—H bond which indicates the formation of a hydrogenated sp^3 C—C carbon network. The intensity of this band is stronger in $UNCD_{550Ar}$ and $UNCD_{550H}$ films. The peak at 773 cm^{-1} is attributed to the out of plane bending vibration of graphite like carbon.[28] A broad band at 1624 cm^{-1} is assigned to sp^2 C—C hybridized (C=C) bonding. The shoulder around 3500 cm^{-1} is ascribed to O—H groups arising due to atmospheric moisture. The other two peaks at 3680 and 3772 cm^{-1} correspond to the symmetric and antisymmetric vibration mode of H_2O molecules.[49] Thus, high adsorption of H_2O molecules is favorable due to high surface energy of $UNCD_{550Ar}$ and $UNCD_{550H}$ films.

3.1.4. Transmission Electron Microscopy Studies. TEM studies can assist in verifying the microstructure and the changes in the hybridized carbon phase in the films deposited in Ar/CH_4 and the $Ar/1.5\% H_2/CH_4$ plasma as a function of T_S. The bright field (BF) TEM image of $UNCD_{550Ar}$ (Figure 4a) along with the selected area electron diffraction (SAED) pattern (inset, Figure 4a) shows that the clusters in the film consist of random/spherical UNCD grains (~5 nm) with uniform size distribution. Grain boundaries of the distinct structure observed in the films are ~1 nm thick. Detailed examination of the SAED patterns reveals the commonly observed (111), (220), and (311) diffraction rings corresponding to the c-diamond of $Fd3m$ symmetry as well as rings corresponding to n-diamond that belong to the *fcc* structure of the diamond phase. Dark field (DF) imaging reveals the shape and size distribution of the grains more clearly. Using the objective/diffraction aperture and selecting two different regions of SAED pattern (red and blue circles in the inner (111) reflection ring of the inset of Figure 4a), the DF-TEM image of $UNCD_{550Ar}$ (Figure 4b) is obtained by superimposing the corresponding DF images. The blue colored features indicate c-diamond grains sizes of about 5−7 nm, while the red colored features correspond to n-diamond grains of sizes of about 10−12 nm.

In the BF-TEM image of $UNCD_{750Ar}$ (Figure 4c), the grains are shown to agglomerate to form large clusters of about a few tens of nanometers in size. The spotty and ring patterns in the SAED image (inset, Figure 4c) arise from the large clusters and randomly oriented diamond grains in the film, respectively. Unlike that observed for the $UNCD_{550Ar}$ films, no extra diffraction ring, besides the (111), (220), and (311) diamond rings, is detected in this SAED pattern. The cluster formation in these films leads to a lesser proportion of grain boundaries in $UNCD_{750Ar}$ as compared with $UNCD_{550Ar}$. The DF-TEM image of $UNCD_{750Ar}$ in Figure 4d shows clearly the existence of anisotropically grown large cluster of grains (red region) of dimensions around 30−80 nm. Hence it can be confirmed that the greater clustering of grains is advanced as a result of the elevated T_S.

The effects that different T_S bring about in the defect structure of the materials are best demonstrated by structure images. Figure 5a and b shows the high-resolution TEM (HRTEM) images corresponding to Figure 4a and c for $UNCD_{550Ar}$ and $UNCD_{750Ar}$, respectively. Figure 5a reveals that
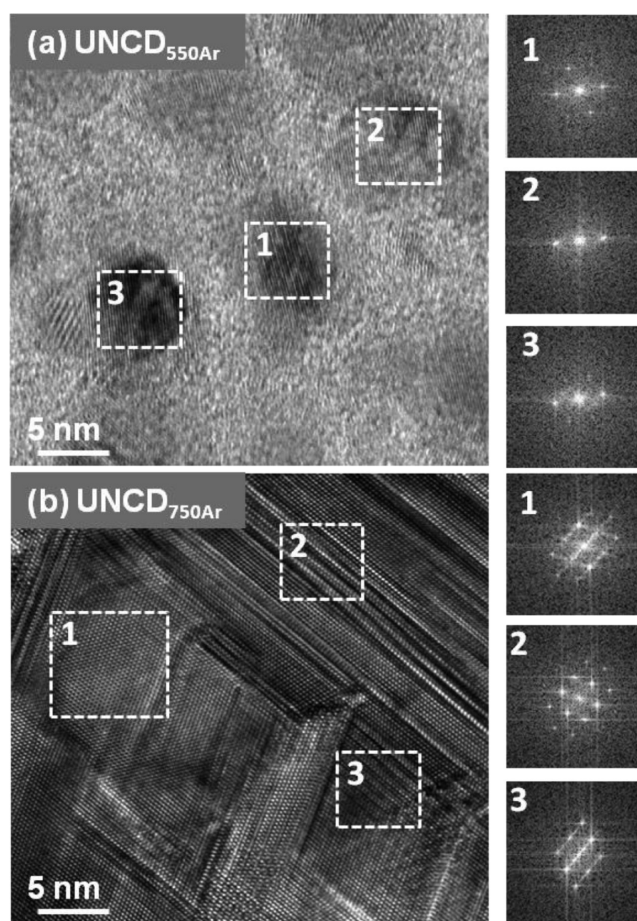
Figure 5. HRTEM image of (a) $UNCD_{550Ar}$ and (b) $UNCD_{750Ar}$. Selections numbered 1−3 show the FT images of different regions in the $UNCD_{550Ar}$ and $UNCD_{750Ar}$ film images.

$UNCD_{550Ar}$ is composed of grains sized around 5 nm. The images numbered 1, 2, and 3 are the Fourier transformed (FT) diffractograms of the regions numbered similarly in the HRTEM images. Large clusters of diamonds are formed when the T_S is raised to 750 °C, as observed in Figure 5b, which also displays the complicated defect structure of $UNCD_{750Ar}$ films. The FT images in Figure 5b show evidence of diamond polytypes which are mostly of hexagonal structure (designated as *n*H).

Figure 6a shows the BF TEM image of $UNCD_{550H}$. Instead of the ultranano equiaxed grains, there exist slightly elongated grain clusters uniformly distributed in the films, similar to those observed for the $UNCD_{750Ar}$ films. It should be noted that in comparison with the grain structure in $UNCD_{550H}$, only small grains are formed in $UNCD_{550Ar}$. Hence the formation of large clusters in $UNCD_{550H}$ may be attributed to the excess H_2 in the reactant gas plasma. Figure 6b shows the DF-TEM image corresponding to Figure 6a, which clearly shows the elongated clusters of grains (blue region) with the size of about 40−80 nm. The SAED pattern (insets, Figures 6a and 6b) contains streaks oriented along the [111] direction, which indicate that the large clusters consist of (111) planar defects (stacking faults). The presence of planar defects implies that the bigger clusters result from the coalescence of the ultranano diamond grains. The TEM image analysis confirms that even at low T_S, the presence of 1.5% H_2 in the Ar/CH_4 plasma can lead to the formation of bigger clusters. The BF-TEM image of $UNCD_{750H}$
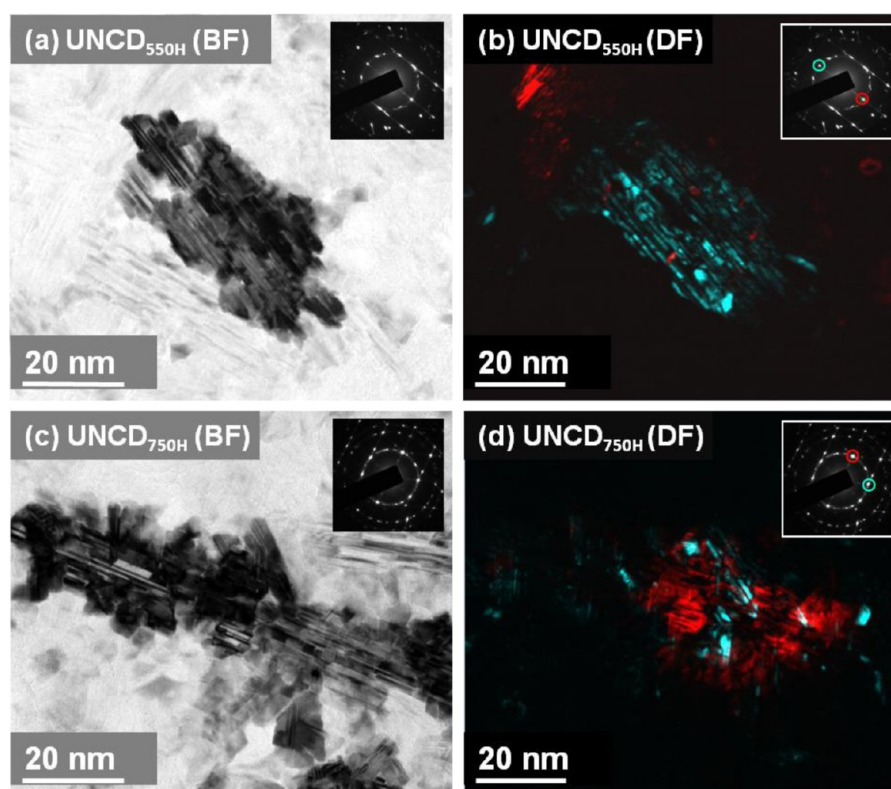
Figure 6. (a) Bright field (BF) and (b) Dark field (DF) TEM images of UNCD$_{550H}$. (c) BF-TEM and (d) DF-TEM images of UNCD$_{750H}$. The insets show the corresponding SAED patterns of each image.

(Figure 6c) shows large cluster formation (60−180 nm) with the grain boundaries almost diminished. The large clusters of grains oriented in different directions overlap one another, forming dendrite geometry. The DF-TEM image (Figure 6d) shows large elongated clustered grains (red region) with size of more than 100 nm and reveals that there are only polytypes of diamond at the high T_S of 750 °C. The presence of streaks in the inner (111) ring also shows that the large dendritic grains are faulted. Moreover, the HRTEM image of UNCD$_{550H}$ (Figure 7a) shows the presence of stacking faults in the films. The FT image of the whole HRTEM image of UNCD film (FT$_0$) suggests a cubic diamond phase contribution. The remaining FT images (square areas 1−3 in Figure 7a) also clearly show the presence of stacking faults in the cubic diamonds. The increase in T_S gives rise to larger size of clusters, endorsing a complicated structure with higher proportion of defects in these clusters, as observed in the HRTEM image of UNCD$_{750H}$ in Figure 7b. The image clearly gives evidence of polymorphs of diamonds and presence of stacking faults observed as the crisscrossed streaks in the images. The corresponding FT images [FT$_0$ and the marked square regions 1−3, Figure 7b] show that the polytypes are hexagonal (nH) type diamonds. As a consequence of large cluster formation, the proportion of grain boundaries is lower while the concentration of stacking faults is higher for UNCD$_{750H}$ in comparison with that of UNCD$_{550H}$.

3.1.5. Optical Emission Spectroscopy Studies. The OES spectra of the Ar/CH$_4$ plasma and Ar/1.5H$_2$/CH$_4$ plasma are recorded (Figure 8a and b) to obtain information of the constituents of the plasma bombarding the substrate. This may also help in understanding the grain growth evolution. The OES spectra for both the series of UNCD films at different T_S

remain the same. The C$_2$ species (Swan band system) are observed at ∼468, ∼516, and ∼563 nm,[50] and the CH species are observed at ∼386 nm. It is observed in the spectra that C$_2$ and CH are the major components in the plasma, which could be the factors contributing to the microstructural evolution of the UNCD films.[50] On the basis of the presence of plasma species, we propose a grain growth model which is discussed in detail shortly.

3.2. Grain Growth Model. The C$_2$ dimer was initially thought to be the lone important player in the grain growth mechanism for UNCD films grown in Ar/CH$_4$ plasma.[51] But recent reports show that apart from the C$_2$ dimers, the competition between H atoms, CH$_3$ radicals, and other C$_1$ species reacting with dangling bonds on the surface determines the renucleation behavior and thereby the morphology of the diamond films.[52−54] Although the mechanisms of the grain growth in UNCD films are still argued upon, it is clear that films grown at low T_S (550 °C) in Ar/CH$_4$ plasma possess ultranano diamond grains with spherical/random geometry and have uniform size distribution with well-defined grain boundaries of considerable thickness.[50] Apparently, the clear grain boundary phase, no matter whether it is pure carbon that is disorderly bonded, as suggested by Gruen et al.,[55] or hydrocarbons (e.g., *t*-PA), as suggested by Ferrari,[42] is formed only at low T_S in Ar/CH$_4$ plasma.

The addition of 1.5% H$_2$ in Ar/CH$_4$ reactant gas content induces the presence of higher content of atomic hydrogen in the plasma. During the initial stages of grain growth the CH species can occupy the grain boundaries while later the carbon−hydrogen bonding configurations form into *t*-PA chains.[56,57] The incoming excess hydrogen can break the *t*-PA bonds by prompting diffusion of existent H in the C−H

3619

dx.doi.org/10.1021/am303144m | *ACS Appl. Mater. Interfaces* 2013, 5, 3614−3624
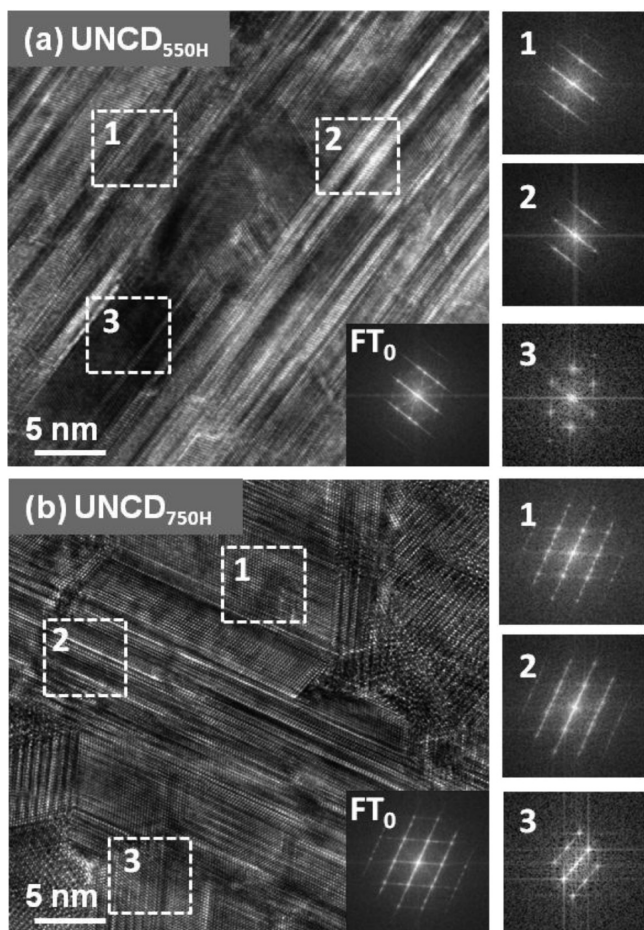
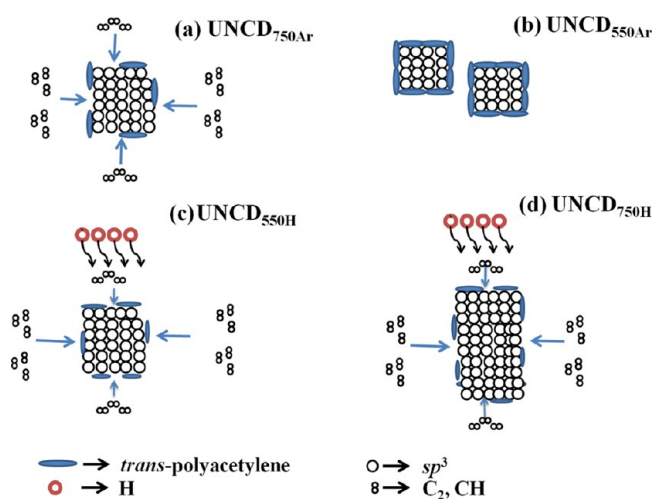**Figure 7.** HRTEM image of (a) UNCD$_{550H}$ and (b) UNCD$_{750H}$. Selections numbered FT$_0$ and 1−3 show the FT images of the whole HRTEM images and different regions, respectively, in the UNCD$_{550Ar}$ and UNCD$_{750Ar}$ film images.

Figure 8. T_S dependence of optical emission spectra of (a) Ar/CH$_4$ plasma and (b) Ar/1.5% H$_2$/CH$_4$ plasma used for growing UNCD films. The C$_2$ and CH species are the major components in both the plasma series.

Figure 9. Schematic grain growth mechanism of films deposited in Ar/CH$_4$ plasma at (a) T_S = 750 °C, (b) T_S = 550 °C and in Ar/1.5% H$_2$/CH$_4$ plasma at (c) T_S = 550 °C and (d) T_S = 750 °C.

bonds.[24] Such kind of breaking and diffusion of H may not be clearly evident in the films deposited in Ar/CH$_4$ plasma as the H generated then may be just ample enough for the CH bond formation without causing excessive bond breaking. Hence the excess atomic hydrogen bombarding may be the cause of extensive breaking of the t-PA bonds thereby leading to preferential etch of the hydrocarbons attached to the diamond surfaces.[35,50] This would lead to a number of dangling carbon bonds which can adhere to the diamond phase, thereby increasing the diamond content in the films.[58] This allows the active carbon in the plasma to further attach to these surfaces, leading to anisotropic growth of the grains, as observed from SEM and TEM images of films grown in Ar/H$_2$/CH$_4$ plasma.[50]

In spite of the existence of such earlier reports on the grain growth of films deposited in different plasma, the importance of T_S in defining the morphology and thereby different properties of the films has not been highlighted. From the present structural and morphological studies using FESEM, Raman spectroscopy, and TEM, a model is proposed for the grain growth process for the films grown in Ar/CH$_4$ and Ar/1.5% H$_2$/CH$_4$ plasmas, highlighting the importance of T_S in defining the morphology of the films. The schematic diagram of grain growth process of the films is depicted in Figure 9. Figure 9a shows the grain growth process of the UNCD$_{750Ar}$ films. Simultaneous to the initial nucleation and growth of the diamond clusters initiated by the sp^3 phase forming

components like C$_2$ dimers and other hydrocarbons (generally depicted as CH$_x$), the t-PA, which is also a hydrocarbon, begins to form and encase these diamond clusters.[50−53] The figure shows that t-PA attaches to the diamond clusters only sparingly. This is because the higher temperature of T_S = 750 °C can destroy the t-PA chains in the grain boundaries, causing desorption of the hydrogen from the sample. It is known that high temperature sustenance of t-PA is difficult, be it high T_S or a high temperature annealing process.[35,59] The lack of t-PA at

the grain boundaries would mean lesser net efficiency of CH to adhere to diamond and uneven passivation of the diamond phase by the t-PA chains and thereby anisotropic grain growth.

Figure 9b draws the grain growth process of UNCD$_{550Ar}$. The low T_S is just sufficient enough to initiate adherence of the diamond grains. The t-PA formed gets attached to the diamond phase, thereby passivating it and hindering further growth of the diamond grain into bigger grains. The Raman analysis in Figure 2c shows that at low T_S the $I_{t-PA}/(I_D + I_G)$ ratio is high and vice versa, indicative of the desorption of a large amount of hydrogen from t-PA in the grain boundaries at high T_S but much lower desorption at low T_S. Further confirmation to this model is that the relative content of t-PA decreases with respect to the diamond phase as shown in Figure 2c, which confirms that the diamond phase increases, which leads to bigger grains, as the t-PA content decreases due to the abstraction of hydrogen from the t-PA caused by the higher T_S. This is visibly evident from the TEM images and analysis in Figures 4 and 5.

Figure 9c presents the schematic diagram of the UNCD$_{550H}$ films. As seen earlier, at lower T_S the diamond clusters formed can be passivated by the t-PA that is formed. But in this case the diamond phase does not get passivated. Here the excess hydrogen in the plasma plays an important role in abstracting the comparatively higher amount of hydrogen in the C–H bonds constituting the t-PA chains by preferential etching than observed for the UNCD$_{nAr}$ films.[35,44] This leads to more diamond grains adhering to each other, leading to larger grain size. In the case of grain growth process for UNCD$_{750H}$ depicted in Figure 9d, both the higher T_S as well as the active excess hydrogen in the plasma contribute toward the desorption of hydrogen from the t-PA chains, thereby resulting in lesser passivation of the diamond clusters, larger extent of diamond grain adherence, ensuing anisotropic growth of the grains. This is proved using the Raman analysis which shows that the net t-PA content in comparison with the other sp^2 phases as well as with respect to the diamond content in the films decreases as shown in Figure 2d.[60]

3.3. Tribological Properties. To judge the validity of the proposed model, this model is used to analyze the tribological properties of UNCD films. Lubrication of diamond or other highly sp^3 bonded carbon based materials occurs due to rehybridization of the carbon bonds on the surface forming a "graphitic" layer.[61,62] This layer can arise when mechanical force acts between the sliding interface which results in the transformation of sp^3-bonds onto an sp^2-hybridized surface. The sp^3-fraction in the film and subsequent transformation of this phase into sp^2-bonding depends on microstructure of the films and tribological sliding contact parameters, respectively. The low friction mechanism in crystalline diamond film is also associated with passivation of surface dangling bonds.[21] It is observed that the morphology and microstructure of UNCD$_{nAr}$ and UNCD$_{nH}$ films are dependent on the plasma chemistry and T_S. The change of chemical structure and microstructure of the films deposited in two different plasma chemistries are important factors which influence the friction behavior.

At the onset, the friction behavior of UNCD films grown in Ar/CH$_4$ plasma at different T_S will be described. The grain size is smaller and grain boundary volume fraction is larger in UNCD$_{nAr}$ films deposited at low T_S as compared to high T_S deposited films. This microstructural behavior is evident by TEM analysis that influences tribological characteristics. The UNCD$_{550Ar}$ film shows a low friction coefficient of 0.015 (curve I, Figure 10a) which increases to 0.1 and 0.13 (curve II and III,
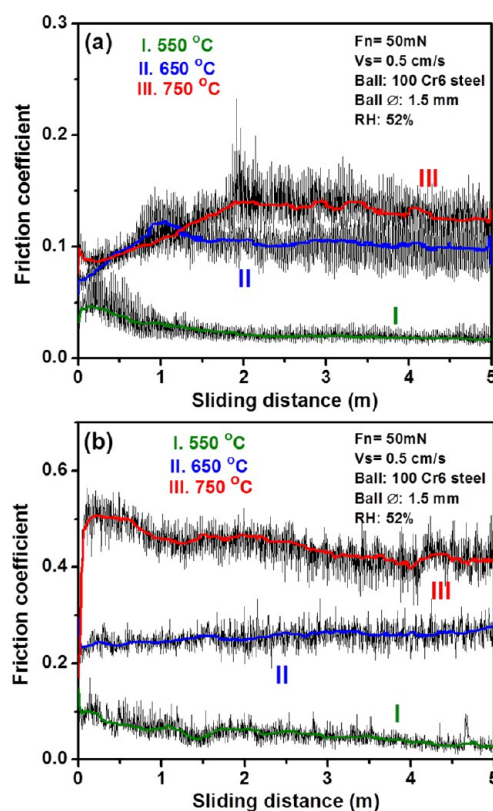
Figure 10. Friction behavior of (a) Ar/CH$_4$ and (b) Ar/1.5% H$_2$/CH$_4$ plasma deposited UNCD films at three different T_S values of 550, 650, and 750 °C.

respectively, Figure 10a) when this film is deposited at high T_S as in the case of UNCD$_{650Ar}$ and UNC$_{750Ar}$ films. Generally, the friction behavior is explained in terms of morphology, microstructure, and chemical characteristics of the grain and grain boundary components.[63,64] The low value of friction coefficient is described by the formation of smaller grains of sp^3-bonded clusters and boundary phases of sp^2-hybridized bonds/a-C and associated t-PA chemical species. The mechanistic aspect causing low friction coefficient (curve I, Figure 10a) is ascribed to large volume of lubricant phase of nanocrystalline graphite and a-C phases present in grain boundaries of UNCD films grown in Ar/CH$_4$ plasma at 550 °C. The presence of these phases is evident from the corresponding Raman spectroscopy and TEM analysis. Generally, the lubricant characteristic of graphite is derived from sheet-like structure where intraplanar carbon atoms are bonded through sp^2-covalent bonds and weak van der Waals forces hold these adjacent basal planes together.[65,66] If the stress is applied, the adjacent sheet of the basal plane easily slides due to low shear resistance which causes dissipation of the low friction coefficient. Therefore, physical characteristic of materials constituted by double bonded carbon molecules exhibit an improved lubrication mechanism. Graphite, hydrogenated diamondlike carbon and hydrogenated crystalline diamond fall into this class of materials.[67,68] However, double bonds are typically more chemically reactive and mechanically unstable compared to single bonds. Therefore, such species are susceptible to tribochemical reactions that normally lead to bond breaking and subsequent bond reconstruction across the interface.[22] Because of this, a material with a higher percentage of sp^2-hybridized bonds may need a higher amount of

passivating chemical species to be present intrinsically in the form of t-PA to saturate such dangling bonds. The t-PA segments, existing in the grain boundary, act as an internal source of H-atoms which passivate the dangling bonds by combining with uncompensated carbon atoms and cause the formation of hydrogen terminated carbon bonds.[69] t-PA favors to form the carboxylated chemical functional groups on the diamond surfaces.

Similarly, in the ambient atmosphere, where H_2O exists, the dangling bonds become hydroxylated forming either —OH or —H terminated surfaces. It also forms C=O, C—O—C, and O—CH_3 functional groups as evident by FTIR analysis (Figure 3). The intensity of these bands is strong in $UNCD_{550Ar}$ and $UNCD_{550H}$ films (Figure 3a and c).These results support the argument that hydroxylic and carboxylic diamond surfaces act to reduce attractive force, which in turn reduces bond formation across the sliding interface and thereby the friction coefficient is decreased.[70] The combination of carboxylated and hydroxylated surfaces are more efficient to reduce the attractive force.[21] The above-mentioned functional groups prevent the formation of covalent C—C bonds across the contact interfaces. In this condition, the dangling carbon covalent bonds are significantly passivated and transformed mostly in the weak van der Waals and hydrogen bonding. This bond is rather weak compared to the covalent C—C bond. The existence of H_2O molecules and the adsorbing capability of the surface consist of a reservoir of such chemical species, which continuously saturate the carbon dangling bonds.

However, when film is deposited at high T_S, the grain is found to grow which causes reduction in the grain boundary fraction. In this respect, the intensity of carboxylated and hydroxylated functional groups on the surface of a diamond film is decreased (Figure 3b and d). At high T_S, the t-PA molecules are unstable and exhibit thermal cracking. When grain boundary volume fraction is reduced and long-range t-PA molecules get generally cracked, the solid lubricant phase of sp^2-hybridized bonds/a-C and t-PA volume fraction decreases and the resulting friction coefficient is found to increase (curves II and III, Figure 10a). The other important factor which causes low friction mechanism in this film is described by mobility of grain boundary sliding relative to grains when a large volume fraction of boundaries are available in UNCD films. The presence of an amorphous boundary phase facilitates grain boundary sliding and improves plasticity.[71] Low resistance of intergranular fracture of the grains appears when grain boundary volume fraction is large and acts as an obstacle in the collision centers of two or more grains. This mechanism is effective when the size of the grain is small and grain boundary volume fraction is large which is constituted by weakly bonded and less densely packed sp^2/a-C and t-PA phases.

Friction behavior of temperature dependent films deposited in Ar/1.5% H_2/CH_4 plasma is quite different as compared to that of films deposited in Ar/CH_4 plasma medium. The friction coefficient increases with T_S and is found to have approximate values of 0.04, 0.25, and 0.45 in $UNCD_{550H}$, $UNCD_{650H}$, and $UNCD_{750H}$ films, respectively, as shown in Figure 10b. Generally, high friction coefficients in these films is associated with large defect induced sp^3 bonded clusters of grains as evident from TEM analysis. These large clusters render grain boundaries immobile. These grain boundaries predominantly consist of sp^2/a-C and t-PA molecules as described in the growth model. The absence of a lubricant phase of sp^2-hybridized bonds/a-C and increase in dangling bonds due to an

insufficient amount of chemically passivating t-PA phase result in increase of friction coefficient. However, low friction coefficient of $UNCD_{550H}$, as shown in curve I of Figure 10b (but higher than that of $UNCD_{550Ar}$), is explained on the basis of chemical behavior of the films as evident from Raman spectra. The I_D/I_G and $I_{t-PA}/(I_D + I_G)$ ratios, shown in Figures 2c and d, are quite similar in variation for the $UNCD_{550Ar}$ and $UNCD_{550H}$ films. The decrease in $I_{t-PA}/(I_D + I_G)$ and the increase of I_D/I_G with T_S hint at higher fraction of sp^2/a-C and t-PA phases at lower T_S. Such a chemical behavior of the $UNCD_{550H}$ film causes a decrease in friction coefficient to a value 0.04. But this value of friction coefficient is higher than that of $UNCD_{550Ar}$ film which has a value of 0.015 (curve I of Figure 10a). Such a low friction coefficient of $UNCD_{550Ar}$ film is associated with the formation of modified microstructural features such as ultranano grains, and their physical and chemical behaviors are discussed above. It is observed that friction coefficient is more sensitive to termination of carbon atoms and dangling bonds than microstructure features. This is valid especially in the case of $UNCD_{550H}$ film. The high T_S, the I_D/I_G ratio of $UNCD_{nH}$ is quite high when compared to that of $UNCD_{nAr}$, is a distinct characteristic associated with sp^2-hybridized bonds/a-C phase fraction inherent to high T_S of film deposited in Ar/1.5% H_2/CH_4 plasma medium. High friction coefficient is also related to crystal structure of the diamond films. The fcc structure observed at low temperature deposited film transforms to polytypes of hexagonal (nH) diamond at high T_S ($UNCD_{750H}$), which consists of large clustered grains with stacking fault defects. The density of uncompensated bonds is higher in the hexagonal structure that contains stacking fault defects. Therefore, it is an energetically higher state compared to fcc cubic structure. This kind of faulty feature causes easy fracture while tribological stress is applied. Such a fracturing event accelerates the density of dangling bonds on the surface, the mechanism invariably resulting in increase in friction coefficient in $UNCD_{650H}$ and $UNCD_{750H}$ films (curves II and III of Figure 10b).

While the existence of grain boundaries of considerable thickness (~1 nm) enhances the tribological properties, there are applications which suffer from the presence of secondary phase (mostly disorder carbons). For example, propagation of acoustic waves and phonons are expected to be significantly scattered that degrades the acoustic wave properties or thermal conductivity of the diamond films. For these applications, eliminating the grain boundary phase is necessary. The above-described results indicate that both increasing the T_S in Ar/CH_4 plasma and/or addition of 1.5% H_2 into Ar/CH_4 plasma are very effective in suppressing the formation of sp^2 along the grain boundaries. In applications which integrate with Si-devices, processes at low T_S are desired. In such cases, utilization of Ar/1.5% H_2/CH_4 plasma is advantageous over Ar/CH_4, as it efficiently eliminates the grain boundary phase at low T_S, while maintaining the grains in an ultranano size, resulting in ultra smooth surface morphology.

4. CONCLUSIONS

UNCD films are grown by MPECVD in gas mixtures of Ar/CH_4 and Ar/1.5% H_2/CH_4 at T_S varying from 550 to 750 °C. TEM examinations reveal that at lower T_S (550 °C) UNCD films from Ar/CH_4 plasma consist of clusters of ultranano diamond grains with well-defined grain boundaries, which is due to the large proportion of CH radical, in conjunction with the C_2 radical. At high T_S (750 °C), the adhering efficiency of

CH radicals onto diamond lattice drops, the nanosize diamond clusters are no longer passivated, and larger diamond clusters of about few tens of nanometers are formed, which also results in the reduction of grain boundaries. In contrast, even at lower T_S, the addition of H_2 in the plasma leads to more cluster formation and grain boundary reduction than that observed in the $UNCD_{nAr}$ films which is due to the weak hydrogen–carbon bonds that cannot passivate the diamond clusters due to desorption of hydrogen from the surfaces. With increase of T_S (750 °C) in $UNCD_{nH}$, the passivation of the diamond phase is suppressed even more efficiently and the growth of elongated clustered grains with diminished grain boundaries is promoted. This is again due to further desorption of hydrogen from the C–H bonds at elevated T_S. The changes in the carbon hybridized phases in the films due to changes in the plasma content and T_S is studied in detail by analyzing the Raman spectra and TEM images. A model is proposed using these results. The model is validated by successfully using it to explain the low and high friction coefficient values of UNCD films. The $UNCD_{550Ar}$ film shows low friction coefficient value of 0.015 and the value being increased when this film is deposited at high T_S as well as the addition of H_2 in Ar/CH_4 plasma. The existence of grain boundaries of considerable thickness (~1 nm) surrounding the ultranano diamond grains and formation of carboxylated and hydroxylated functional group enhances the tribological properties of $UNCD_{550Ar}$ film. This is due to the presence of secondary phases (mostly disorder carbons) in the grain boundaries and passivation of dangling bonds. On the other hand, high friction coefficient for $UNCD_{750H}$ films is also related to crystal structure of the diamond films. The polytypes of hexagonal (nH) diamond at high T_S ($UNCD_{750H}$) consist of large clustered grains with stacking fault defects. The density of uncompensated bonds is higher in the hexagonal structure that contains stacking fault defects. This kind of faulty feature causes easy fracture when tribological stress is applied. Such a fracturing event accelerates the density of dangling bonds on the surface, the mechanism invariably resulting in high friction coefficient of $UNCD_{750H}$ films. Therefore, the variations of functional properties such as friction behavior of UNCD films are found to be sensitive to the changes in microstructure and functional groups on the diamond surface. The investigations based on the tribological properties of UNCD films can make the film be a promising candidate for various applications, mainly in micro/nanoelectro mechanical system (M/NEMS), where low friction is required for high efficiency operation of devices.

■ AUTHOR INFORMATION

Corresponding Author
*E-mail: nhtai@mx.nthu.edu.tw (N.-H.T.) and inanlin@mail.tku.edu.tw (I.-N.L.).

Notes
The authors declare no competing financial interest.

■ ACKNOWLEDGMENTS

■ REFERENCES

(1) Iriarte, G. F. J. Appl. Phys. 2003, 93, 9604–9609.
(2) Bi, B.; Huang, W. S. Diam. Relat. Mater. 2002, 11, 677–680.
(3) Sepulveda-Alancastro, N.; Dean, A. M. Microelectron. Eng. 2004, 73–74,, 435–440.
(4) Auciello, O.; Birrell, J.; Carlisle, J. A.; Gerbi, J. E.; Xiao, X.; Peng, B.; Espinosa, H. D. J. Phys.: Condens. Matter 2004, 16, R539–R552.
(5) Kim, K. H.; Moldovan, N.; Horacio, C. K.; Espinosa, D.; Xiao, X.; Carlisle, J. A.; Auciello, O. Small 2005, 1, 866–874.
(6) Wu, K.; Wang, E. G.; Cao, Z. X.; Wang, Z. L.; Jiang, X. J. Appl. Phys. 2000, 88, 2967–2974.
(7) Yang, W.; Auciello, O.; Butler, J. E.; Cai, W.; Carlisle, J. A.; Gerbi, J. E.; Gruen, D. M.; Knickerbocker, T.; Lasseter, T. L.; Russell, J. N.; Smith, L. M.; Hamers, R. J. Nat. Mat. 2002, 1, 253–257.
(8) Mortet, V.; Elmazria, O.; Nesladek, M.; Assouar, M. B.; Vanhoyland, G.; D'Haen, J.; Olieslaeger, M. D.; Alnot, P. Appl. Phys. Lett. 2002, 81, 1720–1722.
(9) Liu, J.; Grierson, D. S.; Moldovan, N.; Notbohm, J.; Li, S.; Jaroenapibal, P.; O'Connor, S. D.; Sumant, A. V.; Neelakantan, N.; Carlisle, J. A.; Turner, K. T.; Carpick, R. W. Small 2010, 6, 1140–1149.
(10) Lud, S. Q.; Niedermeier, M.; Koch, P. S.; Bruno, P.; Gruen, D. M.; Stutzmann, M.; Garrido, J. A. Appl. Phys. Lett. 2010, 96, 092109.
(11) Bhattacharyya, S.; Auciello, O.; Birrell, J.; Carlisle, J. A.; Curtiss, L. A.; Goyette, A. N.; Gruen, D. M.; Krauss, A. R.; Schlueter, J.; Sumant, A.; Zapol, P. Appl. Phys. Lett. 2001, 79, 1441–1443.
(12) Williams, O. A.; Curat, S.; Gerbi, J. E.; Gruen, D. M.; Jackman, R. B. Appl. Phys. Lett. 2004, 85, 1680–1682.
(13) Joseph, P. T.; Tai, N. H.; Chen, C. H.; Niu, H.; Cheng, H. F.; Palnitkar, U. A.; Lin, I. N. J. Appl. Phys. 2009, 105, 123710.
(14) Joseph, P. T.; Tai, N. H.; Lin, I. N. Appl. Phys. Lett. 2010, 97, 042107.
(15) Joseph, P. T.; Chen, H. C.; Tai, N. H.; Lin, I. N. ACS Appl. Mater. Interfaces 2011, 3 (10), 4007–4013.
(16) Pradhan, D.; Lin, I. N. ACS Appl. Mater. Interfaces 2009, 1, 1444–1450.
(17) Catledge, S. A.; Borham, J.; Vohra, Y. K.; Lacefield, W. R.; Lemons, J. E. J. Appl. Phys. 2002, 91, 5347–5352.
(18) Bogus, A.; Gebeshuber, I. C.; Pauschitz, A.; Roy, M.; Haubner, R. Diam. Relat. Mater. 2008, 17, 1998–2004.
(19) Sharma, N.; Kumar, N.; Sundaravel, B.; Panda, K.; David, W.; Kamarrudin, M.; Dash, S.; Panigrahi, B. K.; Tyagi, A. K.; Lin, I. N.; Raj, B. Tribol. Int. 2011, 44, 980–986.
(20) Panda, K.; Kumar, N.; Panigrahi, B. K.; Polaki, S. R.; Sundaravel, B.; Dash, S.; Tyagi, A. K.; Lin, I. N. Tribol. Int. 2013, 57, 124–136.
(21) Konicek, A. R.; Grierson, D. S.; Gilbert, P. U. P. A.; Sawyer, W. G.; Sumant, A. V.; Carpick, R. W. Phy. Rev. Lett 2008, 100, 235502.
(22) Konicek, A. R.; Grierson, D. S.; Sumant, A. V.; Friedmann, T. A.; Sullivan, J. P.; Gilbert, P. U. P. A.; Sawyer, W. G.; Carpick, R. W. Phys. Rev. B. 2012, 85, 155448.
(23) Holt, K. B.; Ziegler, C.; Zang, J.; Hu, J.; Foord, J. S. J. Phys. Chem. C 2009, 113, 2761–2770.
(24) Yang, W.; Auciello, O.; Butler, J. E.; Cai, W.; Carlisle, J. A.; Gerbi, J. E.; Gruen, D. M.; Knickerbocker, T.; Lasseter, T. L.; Russell, J. N.; Smith, L. M.; Hamers, R. J. Nat. Mat. 2002, 1, 253–257.
(25) Celii, G.; Butler, J. E. Annu. Rev. Phys. Chem. 1991, 42, 643–684.
(26) Morish, A. A.; Pehrsson, P. E. Appl. Phys. Lett. 1991, 59, 417–419.
(27) Lifshitz, Y.; Lee, C. H.; Wu, Y.; Zhang, W. J.; Bello, I.; Lee, S. T. Appl. Phys. Lett. 2006, 88, 243114.
(28) Lee, S. T.; Peng, H. Y.; Zhou, X. T.; Wang, N.; Lee, C. S.; Bello, I.; Lifshitz, Y. Science 2000, 287, 104–106.
(29) Bruno, P.; Benedic, F.; Mohasseb, F.; Silva, F.; Hassouni, K. Thin Solid Films 2005, 482, 50–55.
(30) Correa, E. J.; Wu, Y.; Wen, J. G.; Chandrasekharan, R.; Shannon, M. A. J. Appl. Phys. 2007, 102, 113706.
(31) Csencsits, R.; Gruen, D. M.; Krauss, A. R.; Zuiker, C. Mater. Res. Soc. Symp. Proc. 1996, 403, 291.
(32) Qin, L. C.; Zhou, D.; Krauss, A. R.; Gruen, D. M. Nanostruct. Mater. 1998, 10, 649–660.
(33) Zhou, D.; Gruen, D. M.; Qin, L. C.; McCauley, T. G.; Krauss, A. R. J. Appl. Phys. 1998, 84, 1981–1989.

(34) Jiao, S.; Sumant, A.; Kirk, M. A.; Gruen, D. M.; Krauss, A. R.; Aucciello, O. *J. Appl. Phys.* **2001**, *90*, 118−122.

(35) Pfeiffer, R.; Kuzmany, H.; Knoll, P.; Bokova, S.; Salk, N.; Gunther, B. *Diam. Relat. Mater.* **2003**, *12*, 268−271.

(36) Piazza, F.; Golanski, A.; Schulze, S.; Relihan, G. *Appl. Phys. Lett.* **2003**, *82*, 358−360.

(37) Ferrari, A. C.; Robertson, J. *Phys. Rev. B* **2001**, *64*, 75414.

(38) Birrell, J.; Gerbi, J. E.; Auciello, O.; Gibson, J. M.; Johnson, J.; Carlisle, J. A. *Diam. Relat. Mater.* **2005**, *14*, 86−92.

(39) Xiao, X.; Birrell, J.; Gerbi, J. E.; Auciello, O.; Carlisle, J. A. *J. Appl. Phys.* **2004**, *96*, 2232−2239.

(40) Chen, Q.; Gruen, D. M.; Krauss, A. R.; Corrigan, T. D.; Witek, M.; Swain, G. M. *J. Electrochem. Soc.* **2001**, *148*, E44−E45.

(41) Kuzmany, H.; Pfeiffer, R.; Salk, N.; Gunther, B. *Carbon* **2004**, *42*, 911−917.

(42) Ferrari, A. C.; Robertson, J. *Phys. Rev. B* **2001**, *63*, 121405.

(43) Ferrari, A. C.; Robertson, J. *Phys. Rev. B* **2000**, *61*, 14095.

(44) Ferrari, A. C.; Robertson, J. *Phys. Rev. B* **2001**, *64*, 075414.

(45) Chen, K. F.; Chen, K. C.; Jiang, Y. C.; Jiang, L. Y.; Chang, Y. Y.; Hsiao, M. C.; Chan, L. H. *Appl. Phys. Lett.* **2006**, *88*, 193127.

(46) Huang, B. R.; Yang, Y. K.; Lin, T. C.; Yang, W. L. *J. Nanomater.* **2011**, *2012*, 369763.

(47) Pandey, B.; Pal, P. P.; Bera, S.; Ray, S. K.; Kara, A. K. *Appl. Surf. Sci.* **2012**, *261*, 789−799.

(48) Tang, C. J.; Abe, I.; Vieira, L. G.; Soares, M. G.; Grácio, J.; Pinto, L. J. *Diam. Relat. Mater.* **2010**, *19*, 404−408.

(49) Apatiga, L. M.; Velazquez, R.; Castano, V. M. *Surf. Sci.* **2003**, *529*, 158−162.

(50) Wang, C. S.; Chen, H. C.; Cheng, H. F.; Lin, I. N. *J. Appl. Phys.* **2010**, *107*, 034304.

(51) Zhou, D.; McCauley, T. G.; Qin, L. C.; Krauss, A. R.; Gruen, D. M. *J. Appl. Phys.* **1998**, *83*, 540−543.

(52) May, P. W.; Mankelevich, Yu. A.; Harvey, J. N.; Smith, J. A. *J. Appl. Phys.* **2006**, *99*, 104907.

(53) Rabeau, J. R.; John, P.; Wilson, J. I. B.; Fan, Y. *J. Appl. Phys.* **2004**, *96*, 6724−6732.

(54) May, P. W.; Mankelevich, Yu. A. *J. Phys. Chem. C* **2008**, *112*, 12432−12441.

(55) Gruen, D. M.; Krauss, A. R.; Zuiker, C. D.; Csencsits, R.; Terminello, L. J.; Carlisle, J. A.; Jimenez, I.; Sutherland, D. G. J.; Shuh, D. K.; Tong, W.; Himpsel, F. *J. Appl. Phys. Lett.* **1996**, *68*, 1640−1642.

(56) McNamara, K. M.; Levy, D. H.; Gleason, K. K.; Robinson, C. J. *Appl. Phys. Lett.* **1991**, *60*, 580−582.

(57) Michaelson, Sh.; Hoffman, A. *Diam. Relat. Mater.* **2006**, *15*, 486−497.

(58) Hu, X. J.; Ye, J. S.; Hu, H.; Chen, X. H.; Shen, Y. G. *Appl. Phys. Lett.* **2011**, *99*, 131902.

(59) Ballutaud, D.; Kociniewski, T.; Vigneron, J.; Simon, N.; Girard, H. *Diam. Relat. Mater.* **2008**, *17*, 1127−1131.

(60) Obraztsova, E. D.; Kuznetsov, V. L.; Loubnin, E. N.; Pimenov, S. M.; Pereverzev, V. G. *Nanoparticles in Solids and Solutions*; Fendler, J. H., Dekany, I., Eds.; Kluwer: Dordrecht, 1996.

(61) Gardos, M. N.; Soriano, B. L. *J. Mater. Res.* **1990**, *5*, 2599−2609.

(62) Grillo, S. E.; Field, J. E. *J. Phys. D: Appl. Phys.* **2000**, *33*, 595−602.

(63) Schade, A.; Rosiwal, S. M.; Singer, R. F. *Surf. Coat. Technol.* **2007**, *201*, 6197−6205.

(64) Abreu, C. S.; Oliveira, F. J.; Belmonte, M.; Fernandes, A. J .S.; Silva, R. F.; Gomes, J. R. *Wear* **2005**, *259*, 771−778.

(65) Lancaster, J.; Pritchard, J. *J. Phys. D: Appl. Phys.* **1980**, *13*, 1551−1564.

(66) Lancaster, J.; Pritchard, J. *J. Phys. D: Appl. Phys.* **1981**, *14*, 747−762.

(67) Bowden, F. P.; Young, J. E. *Proc. R. Soc. Lond. A* **1951**, *208*, 444−455.

(68) Andersson, J.; Erck, R. A.; Erdemir, A. *Surf. Coat. Technol.* **2003**, *163−164*, 535−540.

(69) Zilibotti, G.; Righi, M. C.; Ferrario, M. *Phys. Rev. B* **2009**, *79*, 75420.

(70) Gao, G. T.; Mikulski, P. T.; Harision, J. A. *J. Am. Chem. Soc.* **2002**, *124*, 7202−7209.

(71) Voevodin, A. A.; Zabinski, J. S. *Thin Solid Films* **2000**, *370*, 223−231.